Chapter 4

Cross section determination of flux monitor reactions for reactor applications

---

The cross sections were investigated for four important flux monitor reactions namely ^{197}Au(n, 2n)^{196}Au, ^{115}In(n, n')^{115m}In, and ^{232}Th, ^{238}U(n, f)^{97}Zr. The standard NAA method and offline γ ray spectroscopy were utilized for the estimation of cross sections. The proton beam was delivered utilizing the BARC-TIFR accelerator situated in Mumbai, India. The proton beam was targeted on Lithium (Li) target to achieve quasi-monoenergetic neutrons. The comparison was performed with EXFOR data, and various available libraries of nuclear data such as JENDL-4.0, JEFF-3.3, ENDF/B-VIII.0, TENDL-2017, CENDL-3.1, IRDFF II and with the data of TALYS code (v. 1.9). The studied reactions in the present work are extensively used as flux monitor reactions for neutron flux measurements.

Publication related to the present chapter:

Vibhuti Vashi *et al.*, Eur. Phys. J. Plus, **136**:746 (2021). IF: 3.758

4.1 Introduction

Neutron flux has significant importance for a nuclear physics experiment. Some of the examples are stated here: to estimate the appropriate thickness for shielding of the radiation facility, generation of reactor power calculation, transmutation calculations, cross section estimation, and many others. The motivation of this study is to estimate cross section of some important flux monitor reactions which are frequently used for flux estimation in such experiments with better accuracy and provide a new dataset.

It is significant to choose the correct nuclear reaction for flux estimation, and for that reason following are the important criterion to be satisfied by such reactions.

- The product nuclei of the reaction should emit a considerable amount of γ ray so that it gets easier to identify and measure.
- The flux monitor reactions should have lots of cross section data available for nearly the whole energy range.
- The high cross section value requires to obtain a good reaction product.

A list of mostly used flux monitor reactions is tabulated in Table 4.1 from which we have considered four standard flux monitor reactions like ^{197}Au(n, 2n)^{196}Au, ^{115}In(n, n')^{115m}In, and ^{232}Th, ^{238}U(n, f)^{97}Zr.

The chosen reaction ^{197}Au(n, 2n)^{196}Au is not only just extensively used for the measurement of neutron flux but also for high energies dosimetry standards [1, 2]. As the reaction ^{115}In(n, n')^{115m}In has no threshold, this is a favorable reaction for neutron flux estimation in a wide energy range of neuron spectra for fusion and fission reactors [3, 4]. Although the larger and older nuclear data set is available for these reactions, the accuracy and consistency of cross section's data are insufficient. Therefore, the reaction is chosen to provide the data with less error. Indium is also utilized for the construction of control rods which are important to control the neutron flux in nuclear reactors and technology [5].

Table 4.1: Neutron flux monitor reactions are listed with their spectroscopic details [6].

reactions	Isotopic abundance [7] (%)	Threshold energy (E_{th}) [8] (MeV)	Decay mode of Activation Products	Half-life ($\tau_{1/2}$) [9]	γ energy E_γ (keV) [9] Intensity (I_γ) (%)
^{27}Al(n, p)^{27}Mg	100	1.896	100 % β^-	9.46 min	844 (71.8)
^{27}Al(n, α)^{27}Mg	100	3.250	100 % β^-	14.98 h	1369 (100) 2754 (99.944)
^{197}Au(n, 2n)^{196}Au	100	8.114	92.8 % $\varepsilon^+\beta^+$ 72 % β^-	6.183 d	355.73(87) 355.73(87)
^{197}Au(n, γ)^{198}Au	100	0.0	100 % β^-	2.969 d	412 (95.5)
^{115}In(n, n')^{115m}In	95.71	0.0	95 % IT 5 % β^-	4.486 h	336.24(45.83)
^{54}Fe(n, p)^{54}Mn	5.845	0.0	100 % $\varepsilon^+\beta^+$	312.5 d	835 (99.980)
^{56}Fe(n, p)^{56}Mn	91.754	2.966	100 % β^-	2.578 h	847 (98.9)
^{59}Co(n, α)^{56}Mn	100	0.0	100 % β^-	2.578 h	847 (98.9)
^{59}Co(n, p)^{59}Fe	100	0.796	100 % β^-	44.5 d	1099 (56.5)
^{59}Co(n, 2n)^{58}Co	100	10.632	100 % $\varepsilon^+\beta^+$	70.8 d	811 (99.45)
^{58}Ni(n, p)^{58}Co	68.0769	0.0	100 % $\varepsilon^+\beta^+$	70.8 d	811 (99.45)
^{58}Ni(n, 2n)^{57}Ni	68.0769	12.431	100 % $\varepsilon^+\beta^+$	1.503 d	1378 (77.9)
^{232}Th(n, f)^{97}Zr	100	0.0	100 % β^-	16.91 h	743.36(93)
^{238}U(n, f)^{97}Zr	99.2745	0.0	100 % β^-	16.91 h	743.36(93)
^{65}Cu(n, p)^{65}Ni	30.83	1.376	100 % β^-	2.520 h	1481(23.5)
^{65}Cu(n, α)^{62m}Co	30.83	0.188	$\sim$ 100 % β^- $<$ 1 % IT	13.91 min	1173(97.9)
^{93}Nb(n, α)^{90m}Y	100	0.0	100 % IT $<$ 1 % β^-	3.19 h	480 (89.98)
^{93}Nb(n, α)^{9m}Nb	100	8.927	100 $\varepsilon^+\beta^+$	10.15 d	934 (99)

Further, Uranium and Thorium actinide nuclei are chosen for the present study as they have significant dominance in the basic and applied nuclear physics research on nuclear reactions, radiation safety, nuclear structure, dosimetry and the advancement of nuclear reactors [10–14]. The assembled fission fragments during the nuclear reactor operations affect the nuclear fuel by physical and chemical means so we need to know the composition of these fission products [14]. ^{238}U is a key component of nuclear

fuel for all traditional nuclear power plants that include Heavy Water Reactor(HWR), Pressurized Water Reactor (PWR), and Boiling Water Reactor (BWR) [15–17]. ^{232}Th is a fuel used for the Advanced Heavy Water Reactor (AHWR) [18]. Moreover, ^{232}Th, ^{238}U(n, f) reactions are considered flux monitor reactions to estimate the neutron flux [19]. Thus, the precise study of fission cross sections is significant [20–23]. The study is focused on the cross section estimation for ^{232}Th, ^{238}U(n, f) reactions.

The NAA method and offline γ ray spectrometry have been employed for analyzing nuclear data for the selected neutron induced reactions for different neutron energies. The EXFOR data and theoretical model calculations of TALYS (v. 1.9) were used for the experimentally evaluated cross section comparison.

The description of experimental method is portrayed in §4.2. Section 4.3 contains the data analysis part that explains the calculation of average neutron energy and neutron flux utilized to estimate the cross sections of reactions. The detail of suitable tailing corrections utilized for the precise cross sections measurement is included in the same section. The outline of the theoretical model calculations is given in §4.4, and then results and discussions in §4.5.

4.2 Experimental Methodology

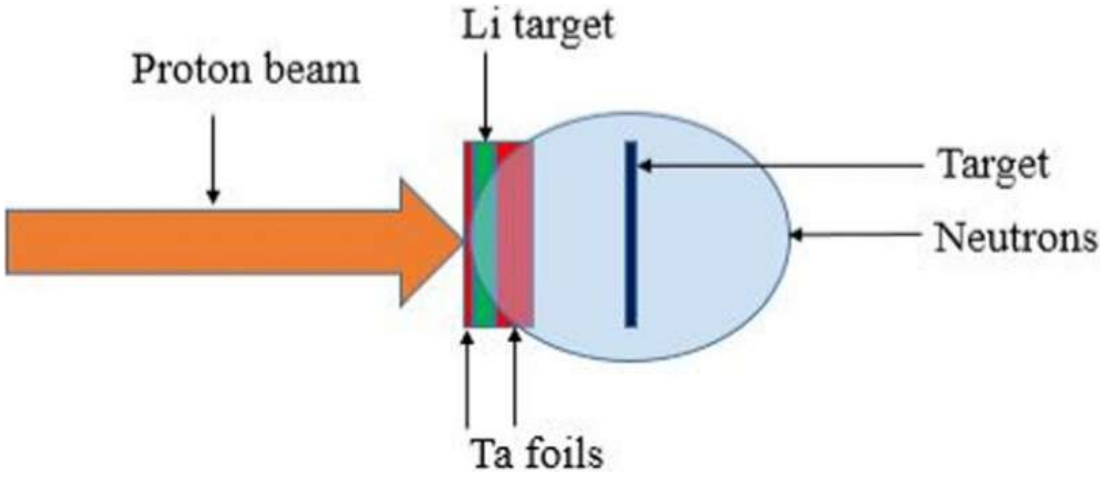

Figure 4.1: A layout of experimental arrangement [24].

The BARC-TIFR pelletron accelerator was utilized for the irradiation experiment using neutrons as incident particles. The NAA-technique and offline γ ray spectroscopy was adopted. A layout of the experimental set up utilized for this study is presented in Fig. 4.1.

Table 4.2: Irradiation experiment details.

	Irradiation I	Irradiation II	Irradiation III	Irradiation IV
Proton Energy (MeV)	18.8	15.0	11.0	7.0
Beam Current (nA)	150	150	120	110
Irradiation time (h:min)	5:00	7:00	16:05	11:15
Au (weight in gm)	-	0.0705	0.0709	-
In (weight in gm)	0.1298	0.0908	0.1358	0.1239
Th (weight in gm)	0.3955	0.2158	0.9005	0.1911
U (weight in gm)	0.3127	0.2884	0.4473	0.2995

Proton beam of four different energy was bombarded on the ^{nat}Li foil of 8.0 mg/cm^2 of thickness. Lithium foil was kept between two Tantalum (Ta) foil. The thickness of the Ta foil at the front is 3.7 mg/cm^2 and the back is 4.12 mg/cm^2. The back Ta foil is required to prevent the hitting of the proton beam directly to the samples. The quasi monoenergetic neutrons were obtained utilizing the ^{7}Li(p, n)^{8}Be reaction. Further, the different natural targets were placed in front of the Ta-Li-Ta assembly. The distance between the targets and the assembly was 2.1 cm. The irradiation that took place with the bombardment of neutrons on the different samples for the suitable irradiation time is mentioned in Table 4.2. The sample weight was determined with the help of a digital micro-balance weighing machine and tabulated in Table 4.2 along with the necessary irradiation detail such as proton energy and beam current.

The ^{115}In(n, n')^{115m}In reaction was utilized as a flux monitor reaction for Au, Th, and U targets. While ^{232}Th(n, f)^{97}Zr reaction for the In target. The thin aluminium foil was used to wrap monitor foils and samples distinctly to avoid cross-contamination between samples. The irradiation port of 6 meters situated at the main beam line of the accelerator was used to carry out the irradiation. To obtain a circular-shaped proton beam, a 6 mm diameter of collimator was utilized. Figure 4.1 represents a

layout of the experimental setup.

After completing the irradiation process, the targets were cooled for a suitable duration to build sufficient activity of gamma rays. Then, the samples were attached to the separate perspex plates and then taken to the HPGe detector which was pre-calibrated with a standard multi gamma ^{152}Eu source. The efficiency curve used for the present calculation is presented in Fig. 4.2. The samples were counted for a considerable duration and the activity is obtained in the form of spectra. A typically recorded γ ray spectra with the gamma lines of the chosen reactions for this study are shown in Fig. 4.3. The detail of the spectroscopic data for the irradiated sample along with chosen gamma ray energies is written in Table 4.3.

The literature [7] was used for the isotopic abundance detail of all samples. The information of threshold energy and Q values are obtained from the Q value calculator of the National Nuclear Data Center (NNDC) [8]. The half-life of product nuclei and its corresponding eminent γ lines are extracted from the literature [9].

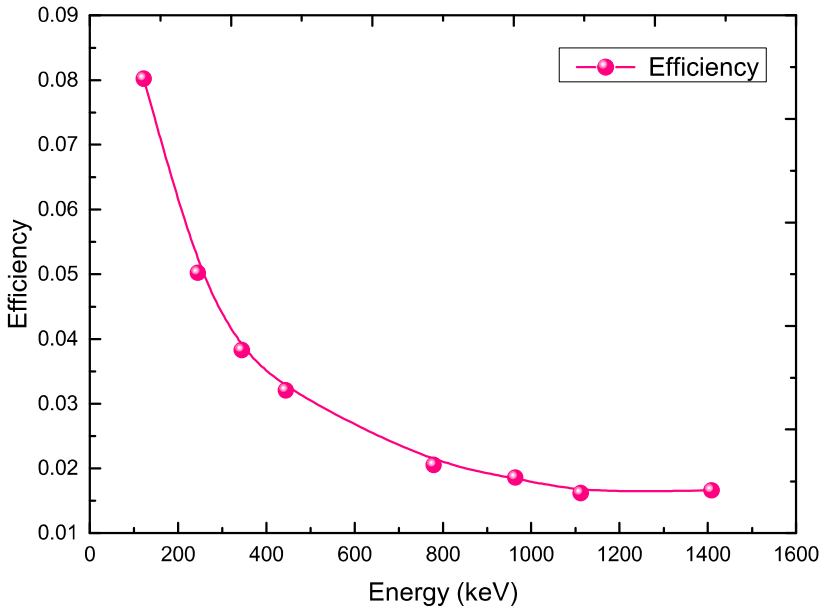

Figure 4.2: Efficiency vs. Energy curve of HPGe detector for ^{152}Eu multi γ point source used in the experiment.

Table 4.3: Spectroscopic details of chosen reactions for the present study.

Reaction	Isotopic Abundance [7] (%)	Threshold Energy [8] (MeV)	Product Nucleus	Half-life [9]	Decay Mode [9]	Eminent γ Energy (keV) [9] Branching Intensity (%)
^{197}Au(n, 2n)^{196}Au	100	8.114	^{196}Au	6.183 d	ϵ : 93.00 % β^- : 7.00 %	355.73(87)
^{115}In(n, n')^{115m}In	95.71	0.0	^{115m}In	4.486 h	IT : 95.00 % β^- : 5.00 %	336.24(45.83)
^{232}Th(n, f)^{97}Zr	100	0.0	^{97}Zr	16.91 h	β^- : 100.00 %	743.36(93)
^{238}U(n, f)^{97}Zr	99.2745	0.0	^{97}Zr	16.91 h	β^- : 100.00 %	743.36(93)

4.3 Analysis of Data

The data collected from the experiment were analyzed in five steps. The first four steps are very important. In the fifth step, the comparison of obtained results was done with the data predicted utilizing nuclear model code: TALYS 1.9.

4.3.1 Activation analysis

The NAA method was utilized for the cross section measurement. This method requires a suitably long half-life of the γ ray emerged from the product nuclei and considerable γ branching abundances. After sufficient cooling, the counts were collected using an HPGe detector via off line mode in the spectrum form. The activation equation given below was used for cross section measurement.

$$\sigma_R = \frac{A_\gamma \lambda (\frac{t_c}{t_r}) e^{\lambda t_w}}{N \epsilon I_\gamma \phi (1 - e^{-\lambda t_c})(1 - e^{-\lambda t_i})} \tag{4.1}$$

where,

σ_R = reaction cross section;

Aγ = number of recognized γ ray count;

λ = decay constant of the residue (s^{-1});

t_c = counting time (s);

t_r = real time (s);

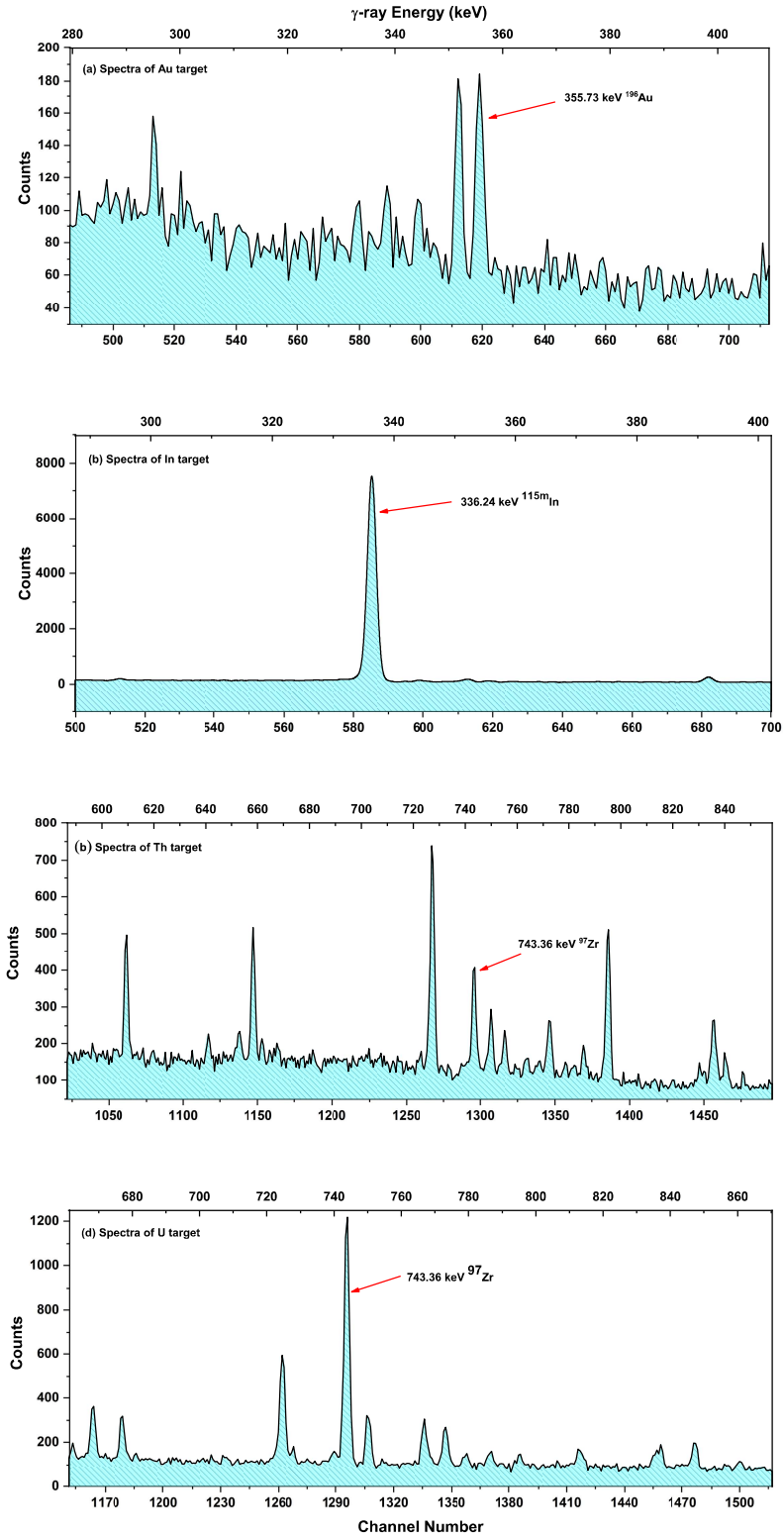

Figure 4.3: Conventionally recorded γ ray spectra using HPGe detector for (a) Au, (b) In, (c) Th, and (d) U samples, respectively.

t_w = cooling time (s);
N = number of target atoms;
ϕ = neutron flux incident on the target (n cm^{-2} s^{-1});
I_γ = branching intensity of γ ray;
ϵ = efficiency of the detector for preferred γ ray.

The activity (A_γ) is calculated for the emitted γ ray of the product nuclide from the γ ray spectra obtained using the HPGe detector. The number of target nuclei was estimated using isotopic abundance and weight of the sample. The spectroscopic data for the chosen reactions are mentioned in Table 4.3. We have considered the term fission yield (Y) in the Eq. 4.1 for the fission cross section calculation.

4.3.2 Average neutron energy calculation

When the proton beam of different energies was bombarded on ^{nat}Li foil, various nuclear reactions occur as per the incident proton energy. The ^{7}Li(p, n)^{7}Be is a key reaction for the quasi-monoenergetic neutrons (n_0) generation in the forward direction. The threshold of the reaction is E_{th} = 1.88 MeV. The generated neutrons of ground and excited state of ^{7}Be merge with the main group of neutrons up to 2.4 MeV of proton energy. The first excited state of ^{7}Be is populated at 0.43 MeV, above 2.4 MeV of proton energy and contributes to the secondary group of neutrons (n_1). The threshold energy of ground state ^{7}Be is 1.881 MeV, and the corresponding ground state neutron energy is E_p-1.881. Further, the threshold energy of the first excited state of ^{7}Be is 2.38 MeV, and the corresponding first excited state neutron energy is E_p-2.38. Below 5 MeV of proton energy, the low energy neutron yield is approximately < 10 % of the ground state and hence monoenergetic neutrons are slightly diminished. Above 6 MeV of proton energy, three body interaction contributes to the production of other neutrons [25, 26]. The neutron energy at 18.8, 15, 11, and 7 MeV of proton energies was obtained using the interpolation technique. Although the lower energy neutrons exist with the main group of neutrons, we can utilize the primary peak for the cross section calculation as it has high neutron energies and flux. The average neutron energy was computed utilizing the Eq. 4.2 and the neutron flux spectra for

18.8, 15, 11, 7 MeV of proton energies were extracted from the literature [25–29] and are given in Fig. 4.4 (a), (b), (c), & (d) respectively.

$$E_{av} = \frac{\int_{E_{ps}}^{E_{max}} E_i \phi_i dE}{\int_{E_{ps}}^{E_{max}} \phi_i dE} \tag{4.2}$$

where,

E_{av} = effective mean energy;

E_i = energy interval;

ϕ_i = neutron flux;

E_{ps} = peak forming start neutron energy;

E_{max} = maximum neutron energy.

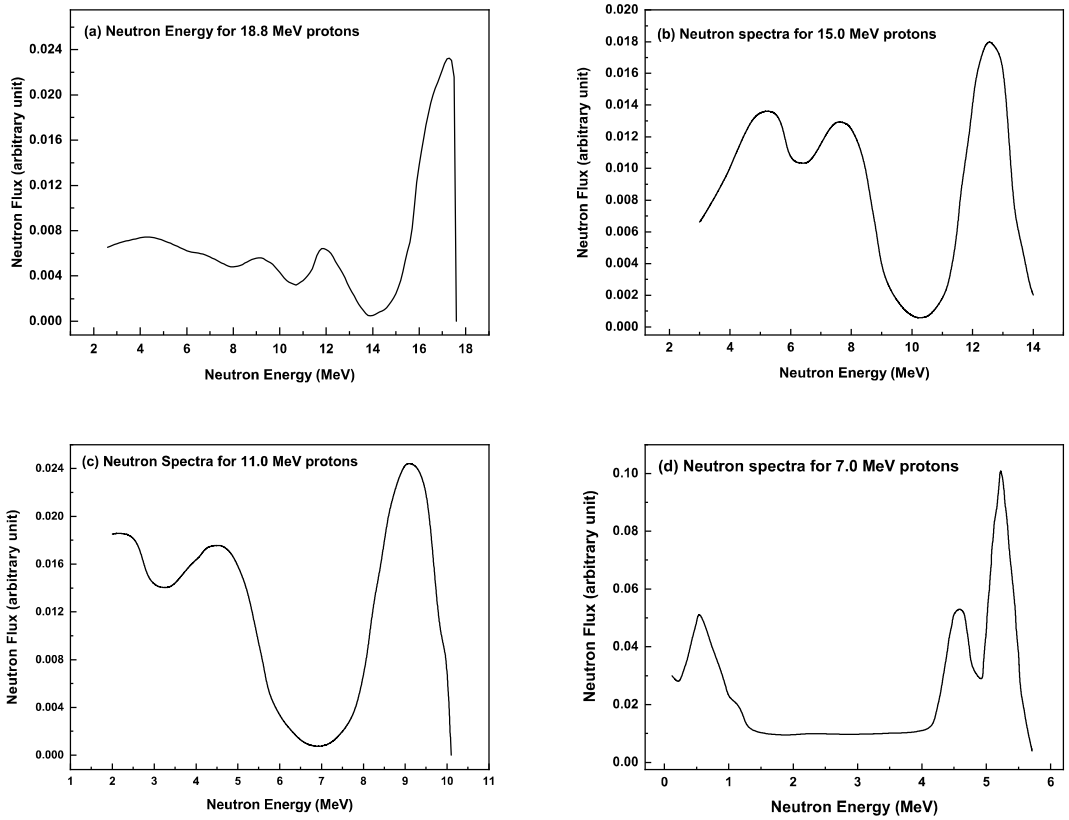

Figure 4.4: (a)-(d) The neutron flux spectra obtained using ^{7}Li(p,n) reaction for (a) 18.8, (b) 15.0, (c) 11.0, and (d) 5.0 MeV of proton energies.

4.3.3 Average neutron flux calculation

The neutron flux is crucial for the cross section estimation and it is taken from the neutron spectra presented in Fig. 4.4. In the present study, two different flux monitor reactions, ^{115}In(n, n')^{115m}In and ^{232}Th(n, f)^{97}Zr were utilized for neutron flux estimation and their spectroscopic details are available in Table 4.3. The spectrum averaged cross sections were calculated by utilizing the latest data accessible from the EXFOR database for ^{115}In(n, n') [30–33] and ^{232}Th(n, f) [34–37] reactions. These average reaction cross sections were utilized for the evaluation of incident neutron flux. The spectrum averaged neutron cross sections were computed using Eq. 4.3 and neutron flux using Eq. 4.4.

$$\sigma_{av} = \frac{\int_{E_{th}}^{E_{max}} \sigma_i \phi_i dE}{\int_{E_{th}}^{E_{max}} \phi_i dE} \tag{4.3}$$

where,
σ_{av} = spectrum averaged cross-sections;
σ_i = cross-section at energy E_i for flux monitor reaction extracted from EXFOR [30–32, 34–37];
ϕ_i = neutron flux for energy E_i;
E_{max} = maximum peak energy for neutrons;
E_{th} = threshold energy.

$$\phi = \frac{A_\gamma \lambda (\frac{t_c}{t_r}) e^{\lambda t_w}}{N \epsilon I_\gamma \sigma_{av} (1 - e^{-\lambda t_i})(1 - e^{-\lambda t_c})} \tag{4.4}$$

All the parameters of the above equation are the same as in Eq. 4.1 except σ_{av}.

The neutron flux was measured from the monitor reactions and can be utilized for the evaluation of the cross sections for the chosen reaction. For the calculation of neutron flux using ^{232}Th(n, f)^{97}Zr flux monitor, the fission yield was considered. The spectrum averaged reaction cross sections and neutron flux values were consumed from the ref. [24].

4.3.4 Low energy neutron correction

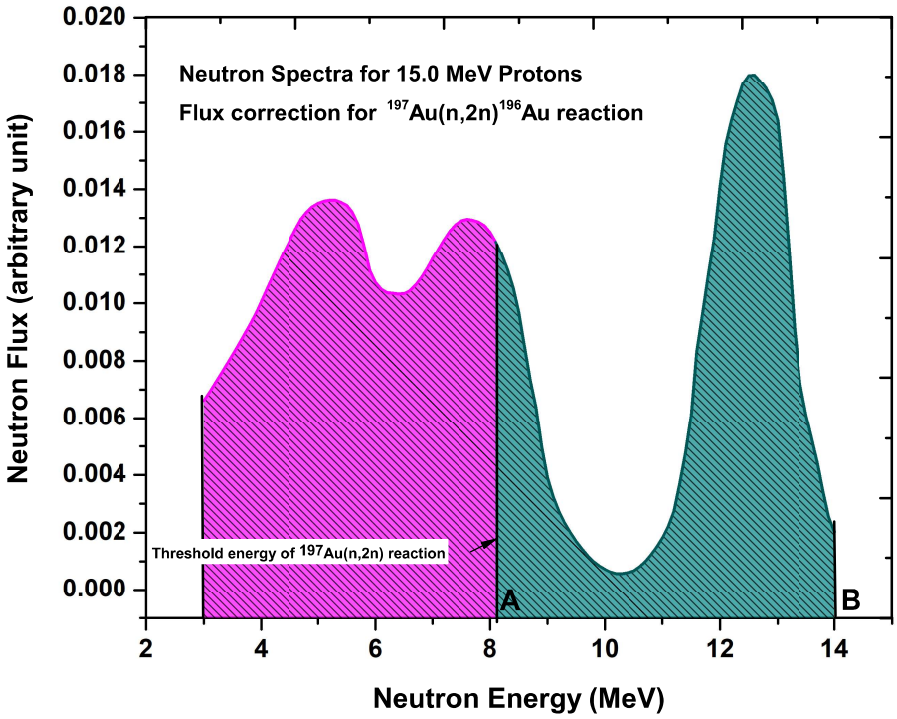

Figure 4.5: Neutron flux correction for ^{197}Au(n, 2n)^{196}Au reaction having 8.114 MeV of threshold energy labelled by **A** and maximum neutron energy labelled by **B**.

The neutron source generated in the laboratory with the accelerator facility is barely monoenergetic due to the low energy neutrons present in nearly all cases. These neutrons are exceeding the primary group of neutrons either by the secondary reactions or neutron scattering occurring in the laboratory or via excitation of the multiple levels and various open channels, as discussed in the §4.3.2. The contribution of the secondary neutrons along with the primary neutrons should be removed for the accurate cross section measurement. The main group of neutrons have a well defined broad peak at higher energy region with higher neutron flux compared to secondary neutrons therefore low energy neutrons can be easily removed using tailing correction. Neutron flux for the capture reaction can be measured easily as total neutron flux

can be used for it but for the reactions with threshold, the neutron flux correction is required. The presently studied ^{197}Au(n, 2n)^{196}Au reaction having 8.114 MeV of threshold energy and the tailing correction was performed using the spectral indexing technique described in the literature [29].

Tailing correction can be performed by removing neutron flux from minimum to threshold energy and by taking the area under the curve of the neutron flux. So, to calculate the final cross section, the area under the curve of neutron spectra requires threshold energy (E_{th}) labelled as "A" to the maximum neutron energy "B" as presented in Fig. 4.5. Further, to remove the averaged cross section from E_{th} to the energy where peak formation is beginning (E_{ps}), the theoretical calculations were performed utilizing TALYS-1.9 to achieve the cross sections as a function of neutron energies. These cross sections were convoluted at different energies with the neutron flux taken from Fig. 4.4 (a)-(d) for different neutron energies. The spectrum averaged reaction cross sections were estimated from minimum to threshold energy and subtracted from the data obtained using Eq. 4.1. Hence, the actual cross section value for the present reaction is obtained at the spectrum-averaged neutron peak energy.

4.4 TALYS-1.9 calculations

TALYS is a versatile code extensively utilized for the simulation of basic experiments and the nuclear data generation for several applications [38]. This code predicts the nuclear data employing different theoretical approaches to nuclear physics [39]. The detailed idea of TALYS is presented in Chapter 3. The code can simulate the nuclear reaction data for neutral and light charged particle projectiles and targets heavier than Carbon nuclei within MeV of energy range. The input parameters are utilized from the RIPL library of IAEA [40]. The various nuclear models are employed in TALYS namely, direct reactions, compound and pre-compound, and fission.

Six NLD models of TALYS and the detail of the parameters are mentioned in the manual of TALYS [41] and have been used for the present study. The calculations

were performed using all NLD models from ldmodel 1 to ldmodel 6 of TALYS (v. 1.9) but the best fit among all the models has been chosen for ^{197}Au(n, 2n)^{196}Au, ^{115}In(n, n')^{115m}In reactions and presented in Fig. 4.6 and 4.7, respectively.

A systematic study of nuclear fission is challenging to accomplish as per the manual of TALYS. Many adjustable input parameters have been used in TALYS to achieve very satisfactory fits of fission data. ^{232}Th(n, f)^{97}Zr and ^{238}U(n, f)^{97}Zr reaction cross sections were calculated by utilizing the existing sample file of TALYS-1.9. The obtained cross sections were simulated with the EXFOR and ENDF data, and shown in Fig. 4.8 and 4.9, respectively.

4.5 Results & Discussion

The prime motivation of the work is to report cross section data for the enhancement of the nuclear data libraries for the nuclear physics applications. The nuclear data for the chosen reactions are important as these reactions are extensively used as the flux monitor reactions for neutron flux estimation and other nuclear reactor applications. The theoretical predictions were carried out utilizing the TALYS code to validate the present data. The cross sections were determined for the ^{197}Au(n, 2n)^{196}Au, ^{232}Th(n, f)^{97}Zr, and ^{238}U(n, f)^{97}Zr reactions for different neutron energies and simulated with the EXFOR data and other evaluated nuclear data libraries namely JENDL-4.0, JEFF-3.3, ENDF/B-VIII.0, CENDL-3.1, TENDL-2017, and IRDFF II. The cross sections were also determined for ^{115}In(n, n')^{115m}In reaction

Table 4.4: Major uncertainties included in the measured cross section results.

Parameter	Limit ($\leq$)
count rate	$\leq$ 4.5 %
Self-absorption	$\leq$ 0.2 %
Neutron flux	$\leq$ 6 %
Mass	$\leq$ 0.001 %
Efficiency calibration	$\leq$ 3 %

and simulated with the theoretical predictions of TALYS, and the EXFOR data. The major uncertainties in measured cross sections of the studied reactions are given in Table 4.4.

(a) ^{197}Au(n, 2n)^{196}Au reaction

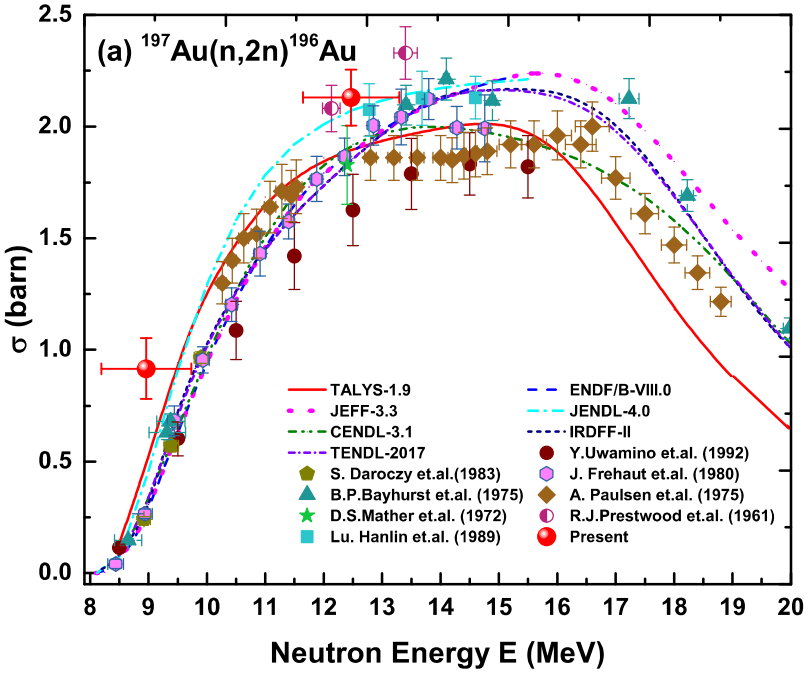

Figure 4.6: Experimentally measured activation cross section data of ^{197}Au(n, 2n)^{196}Au reaction compared with existing data of different libraries and predicted data of TALYS (v. 1.9).

The cross sections were estimated for this reaction for 12.47 ± 0.83 and 8.96 ± 0.77 MeV of average neutron energies and presented in Fig. 4.6. As the threshold energy of the reaction is 8.114 MeV, it is not possible to measure cross sections below this energy. Figure 4.6 depicts that the data of the JENDL-4.0 library is in good resemblance with the presently measured data of 12.47 ± 0.83 MeV of neutron

energy. Theoretical predictions of the TALYS-1.9 code are lower than the measured cross section data for both energies. However, the cross section value of 8.96 ± 0.77 MeV neutron energy is bit higher than the value of theoretical codes and data library.

(b) ^{115}In(n, n')^{115m}In reaction

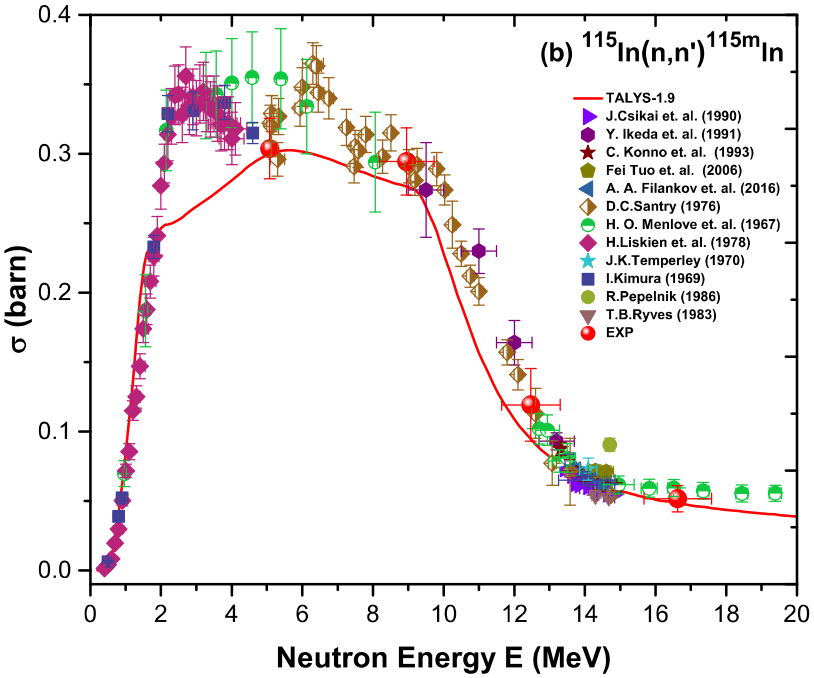

Figure 4.7: Experimentally measured activation cross sections of ^{115}In(n, n')^{115m}In reaction compared with the EXFOR data and data obtained from TALYS (v. 1.9).

The cross sections of this reaction were determined for four different energies 16.63 ± 0.95, 12.47 ± 0.825, 8.96 ± 0.77, and 5.08 ± 0.165 MeV of neutron energies and presented in Fig. 4.7. All the presently estimated data points shows good resemblance with the theoretical predictions of TALYS for the present case. The cross section value corresponding to 16.63 ± 0.95, 12.47 ± 0.825, and 5.08 ± 0.165 MeV of neutron energies is compatible with the literature data of ref. [42]. The cross section of neutron

energy 16.63 ± 0.95 MeV is well-matched with the data of ref. [43] as well as with the theoretical prediction of TALYS.

(c) ^{232}Th(n, f)^{97}Zr reaction

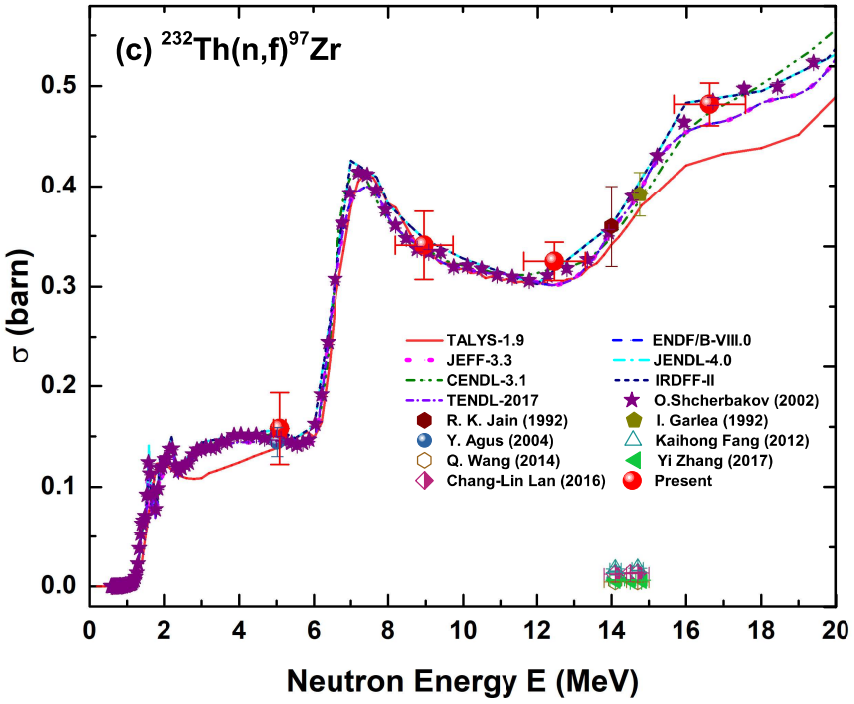

Figure 4.8: Experimentally measured activation cross section data of ^{232}Th(n, f)^{97}Zr reaction compared with existing data of different libraries and predicted data of TALYS.

The cross sections for ^{232}Th(n, f)^{97}Zr reaction were measured at 16.63 ± 0.95, 12.47 ± 0.825, 8.96 ± 0.77, and 5.08 ± 0.165 MeV of neutron energies and plotted in Fig. 4.8. The cross section value for 16.63 ± 0.95 MeV of neutron energy is comparable with the EXFOR database [44] and with available evaluated data libraries. Theoretical predictions of TALYS is slightly underestimated by the present cross-

section value for 16.63 ± 0.95 MeV of neutron energy. The cross section values of the other three energies shows better agreement with all the data libraries, and with the data of TALYS.

(d) ^{238}U(n, f)^{97}Zr reaction

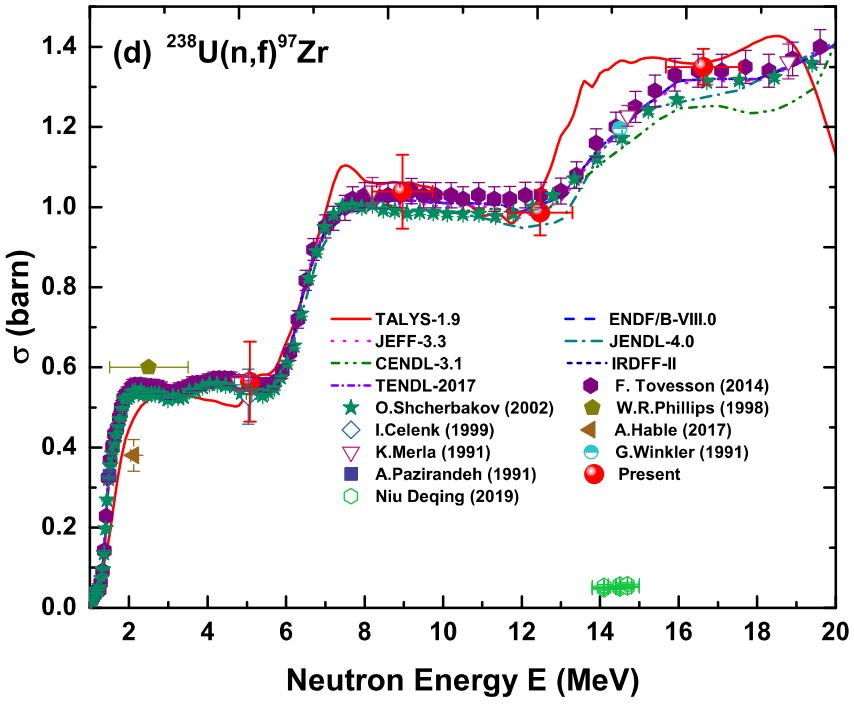

Figure 4.9: Experimentally measured activation cross section data of ^{238}U(n, f)^{97}Zr reaction compared with existing data of different libraries and predicted data of TALYS.

The cross sections of this reaction were estimated at 16.63 ± 0.95, 12.47 ± 0.825, 8.96 ± 0.77, and 5.08 ± 0.165 MeV of neutron energies and shown in 4.9. The estimated cross section data are in better resemblance with the values of all data libraries and with theoretical cross sections of TALYS.

Overall, it is observed that theoretical predictions of TALYS shows better agree-

ment with the presently measured cross section data of all reactions and the measured values of these reactions are shown in Table 4.5.

4.6 Summary & Conclusion

The present work is a contribution to nuclear technology development concerning better data for nuclear monitor reaction cross-sections. These are the much-needed data for the exact estimation of neutron flux viz. nuclear power. The cross sections were measured at different neutron energies for the reactions such as ^{197}Au(n, 2n)^{196}Au, ^{115}In(n, n') ^{115m}In, ^{232}Th(n, f)^{97}Zr, and ^{238}U(n, f)^{97}Zr which are widely used as flux monitor to calculate the neutron flux in NAA-technique. The cross sections were measured using NAA-technique followed by off-line γ ray spectroscopy with the standard tailing corrections [25]. The neutron flux was calculated using ^{115}In(n, n')^{115m}In flux monitor for ^{197}Au(n, 2n)^{196}Au, ^{232}Th(n, f)^{97}Zr, and ^{238}U(n, f)^{97}Zr reactions and ^{232}Th(n, f)^{97}Zr reaction was utilized as a flux monitor for ^{115}In(n, n')^{115m}In reaction. The spectrum averaged neutron energy and precise neutron flux measurements have been performed. It is essential to measure cross sections for these reactions as the available experimental data are very old. The cross sections of ^{115}In(n, n')^{115m}In, ^{232}Th(n, f)^{97}Zr, and ^{238}U(n, f)^{97}Zr reactions are reported for four different energies such as 16.63 $\pm$ 0.95, 12.47 $\pm$ 0.825, 8.96 $\pm$ 0.77 and 5.08 $\pm$ 0.165 MeV. For ^{197}Au(n, 2n)^{196}Au reaction, the cross sections are reported at 12.47 $\pm$ 0.825, 8.96 $\pm$ 0.77 MeV of energies. Figures shows that the measured cross section data follow the general trend of the available experimental results and theoretical predictions of TALYS-1.9. Furthermore, theoretical calculations were carried utilizing the TALYS code for all the reactions. All the experimental measurements were compared with the result of theoretical predictions and with the literature data which are extracted from the EXFOR data library. It may be concluded that the present data shows an overall satisfactory agreement with the EXFOR database and also with theoretical predictions.

Table 4.5: Comparison of the presently measured experimental data with the theoretical predictions of TALYS 1.9.

Cross sections for ^{197}Au(n, 2n)^{196}Au reaction.

Neutron Energy (MeV)	Measured Cross-section (barn)	TALYS-1.9 (barn)
12.47 ± 0.83	2.126 ± 0.124	1.899
8.96 ± 0.77	0.916 ± 0.136	0.489

Cross sections for ^{115}In(n, n')^{115m}In reaction.

Neutron Energy (MeV)	Measured Cross-section (barn)	TALYS-1.9 (barn)
16.63 ± 0.95	0.0517 ± 0.0094	0.0483
12.47 ± 0.83	0.1193 ± 0.0262	0.0950
8.96 ± 0.77	0.2945 ± 0.0243	0.2770
5.08 ± 0.17	0.3038 ± 0.0216	0.2999

Cross sections for ^{232}Th(n, f)^{97}Zr reaction.

Neutron Energy (MeV)	Measured Cross-section (barn)	TALYS-1.9 (barn)
16.63 ± 0.95	0.482 ± 0.021	0.428
12.47 ± 0.83	0.325 ± 0.019	0.302
8.96 ± 0.77	0.341± 0.034	0.339
5.08 ± 0.17	0.158± 0.036	0.140

Cross sections for ^{238}U(n, f)^{97}Zr reaction.

Neutron Energy (MeV)	Measured Cross-section (barn)	TALYS-1.9 (barn)
16.63 ± 0.95	1.356 ± 0.044	1.356
12.47 ± 0.83	0.986 ± 0.057	1.031
8.96 ± 0.77	1.038 ± 0.092	1.060
5.08 ± 0.17	0.564 ± 0.099	0.548

Bibliography

[1] R. Raut *et al.*, J. Phys. Conf. Ser. **312**, 062008 (2011).

[2] L. R. Greenwood and A. L. Nichols, "Review the requirements to improve and extend the IRDF library (International reactor dosimetry file (IRDF-2002))", IAEA Report, INDC(NDS)-0507 (2007).

[3] Fei Tuo *et al.*, App. Rad. and Iso. **64**, 910-914 (2006).

[4] T. B. Ryves *et al.*, J. Phys. G: Nucl. Phys. **9**, 1549-1564 (1983).

[5] D. A. Petti, Nucl. Technol. **84**, 128 (1989).

[6] Cezar Ciprian Negoita, Measurement of Neutron Flux Spectra in a Tungsten Benchmark by Neutron Foil Activation Method (2004).

[7] K. J. R. Rosman and P. D. P. Taylor, Pure Appl. Chem. **70**, 217 (1998).

[8] `http://www.nndc.bnl.gov/qcalc/index.jsp`, retrieved on 11 August 2019.

[9] `http://www.nndc.bnl.gov/nudat2/indxdec.jsp`, retrieved on 21 August 2019.

[10] A. Turkevich and J. B. Niday, Phys. Rev. C **84**, 52-60 (1951).

[11] E. T. Cheng *et al.*, Fusion Eng. Des. **10**, 231-242 (1989).

[12] D. V. Markovskij, Fusion Eng. Des. **51-52**, 695-700 (2000).

[13] M. Igashira and T. Ohsaki, Prog. Nucl. Energy **40**, 555-560 (2002).

[14] X. J. Sun *et al.*, Commun. Theor. Phys. **62**, 711 (2013).

[15] Y. W. Lee and M. S. Yang, Nucl. Mater. J **178** (2-3), 217-226 (1991).

[16] T. Mochida *et al.*, Prog. Nucl. Energy **32** (3-4), 579-586 (1998).

[17] Y. Huseyin, Ann. Nucl. Energy **30**, 413-436 (2003).

[18] R. K. Sinha and A. Kakodkar, Nucl. Eng. Des. **236** (7), 683-700 (2006).

[19] Zhimin Wang *et al.*, Phys. Rev. C **92**, 044601 (2015).

[20] M. Sin *et al.*, Phy. Rev. C **74**, 014608 (2006).

[21] V. M. Maslov, Phys. Lett. B **649**, 376 (2007).

[22] Chang-Lin Lan *et al.*, Eur. Phys. J. A **52**:345 (2016).

[23] Niu Deqing *et al.*, Rad. Phy. and Chem. **158**, 175-179 (2019).

[24] Rajnikant Makwana *et al.*, Phys. Rev. C **96**, 024608 (2017).

[25] C. H. Poppe *et al.*, Phys. Rev. C **14**, 438 (1976).

[26] J. D. Anderson, C. Wong, and V. A. Madsen, Phys. Rev. Lett. **24**, 1074 (1970).

[27] P. M. Prajapati *et al.*, Eur. Phys. J. A **48**, 1 (2012).

[28] M. W. Mcnaughton *et al.*, Nucl. Instrum. Methods **130**, 555 (1975).

[29] D. L. Smith *et al.*, Corrections for Low Energy Neutrons by Spectral Indexing, retrieved from `https://www.oecdnea.org/science/docs/2005/nsc-wpec-doc2005-357.pdf`.

[30] G. Loevestam *et al.*, Nucl. Instrum. Methods Phys. Res. Sect. A **580**, 1400 (2007).

[31] Y. Agus, I. Celenk, and A. Ozmen, Radiochim. Acta **92**, 63 (2004).

[32] M. S. Uddin *et al.*, Radiochim. Acta **101**, 613 (2013).

[33] A. A. Lapenas, Neutron (Riga, USSR, Zinatne, 1975), p. 80.

[34] O. A. Shcherbakov *et al.*, in International Seminar on Interactions of Neutrons with Nuclei, Dubna, Russia, Vol. **9,** p. 257 (2001).

[35] R. K. Jain, Pramana **49**, 515 (1997).

[36] I. Garlea *et al.*, Rev. Roum. Phys. **37**, 19 (1992).

[37] F. Manabe *et al.*, Fac. of Engineering, Tohoku Univ. Tech. Report **52** (Issue 2) 97 (1988).

[38] A. Koning, S. Hilaire, and S. Goriely, TALYS-1.9 - A Nuclear Reaction Program, User Manual, 1^{st} edn (NRG, Westerduinweg, 2017).

[39] N. Dzysiuk *et al.*, Phys. Rev. C **81**, 014610 (2010).

[40] R. Capote *et al.*, Nucl. Data Sheets **110**, 3107 (2009).

[41] S. Hilaire *et al.*, Phys. Rev. C **86**, 0643177 (2012).

[42] D. C. Santry and J. P. Butler, Can. J. Phys. **54** (1976).

[43] H. O. Menlove *et al.*, Phys. Rev. **163**, 4 (1967).

[44] Cross Section Information Storage and Retrieval System (EXFOR), IAEA,Vienna,Austria. `https://wwwnds.iaea.org/exfor/`